NIH Public Access
Author Manuscript
*J Opt Soc Am A Opt Image Sci Vis*. Author manuscript; available in PMC 2009 January 1.

Published in final edited form as:
*J Opt Soc Am A Opt Image Sci Vis*. 2008 October ; 25(10): 2571–2581.

# Monte Carlo modeling of spatial coherence: free-space diffraction

**David G. Fischer**[1,*], **Scott A. Prahl**[2], and **Donald D. Duncan**[3]

1*NASA Glenn Research Center, 21000 Brookpark Road, Cleveland, Ohio 44135, USA*

2*Oregon Medical Laser Center, Providence St. Vincent Medical Center, 9205 SW Barnes Road, Portland, Oregon 97225, USA*

3*Department of Biomedical Engineering, Oregon Health & Science University, 3303 SW Bond Avenue, Portland, Oregon 97239, USA*

## Abstract

We present a Monte Carlo method for propagating partially coherent fields through complex deterministic optical systems. A Gaussian copula is used to synthesize a random source with an arbitrary spatial coherence function. Physical optics and Monte Carlo predictions of the first- and second-order statistics of the field are shown for coherent and partially coherent sources for free-space propagation, imaging using a binary Fresnel zone plate, and propagation through a limiting aperture. Excellent agreement between the physical optics and Monte Carlo predictions is demonstrated in all cases. Convergence criteria are presented for judging the quality of the Monte Carlo predictions.

## 1. INTRODUCTION

The propagation of partially coherent light through optical systems is important in many applications, most notably imaging, metrology, and spectroscopy. In general, the coherence properties of light change on propagation, even in free space [1]. For simple systems, such as two-dimensional diffracting structures and weakly scattering media, the propagation of partially coherent light can be treated analytically, for both the deterministic and random cases [1–5]. For more complex systems, however, there are no closed-form solutions.

In many cases, the propagation of light through complex structures, such as highly scattering media, can be treated numerically using Monte Carlo techniques [6–8], which allow for the specification of difficult boundary conditions in a straightforward manner. This approach is based on the radiative transfer equation (RTE) [9,10], which assumes incoherent light propagation, although there have been attempts to incorporate phase information so that coherence affects can be studied [11,12]. It should be pointed out that although the Monte Carlo method is a statistical method (involving statistical sampling), it is typically employed to study light transport through *deterministic* systems. It is only due to the complexity of the system and its associated structures that a statistical treatment must be adopted, much like in the case of statistical mechanics. The generalization of the RTE to randomly inhomogeneous media has also been studied, both for the specific intensity as well as the intensity correlation function [13]; however, only approximate solutions have been obtained in some limited cases. Recently, the use of Monte Carlo methods to study the propagation of partially coherent light has also been investigated [14]. In this case, an analytic correlation function was employed to weight various ray trajectories and the intensity in the observation plane was determined.

*Corresponding author: cdfischer@roadrunner.com.

NIH-PA Author Manuscript
NIH-PA Author Manuscript
NIH-PA Author Manuscript

NIH-PA Author Manuscript
NIH-PA Author Manuscript
NIH-PA Author Manuscript



In this paper, we demonstrate a Monte Carlo approach for propagating partially coherent fields through complex deterministic diffracting structures. Propagation through scattering media, such as human tissue, will be covered in a later paper. As many such structures are separable in the transverse dimensions, we treat the two-dimensional problem (one transverse dimension and the axial dimension). For synthesizing a random source with an arbitrary spatial coherence function we introduce the use of a Gaussian copula. Physical optics and Monte Carlo predictions of the first- and second-order statistics of the field are shown for coherent and partially coherent sources for free-space propagation, imaging using a binary Fresnel zone plate, and propagation through a limiting aperture. Excellent agreement between the physical optics and Monte Carlo predictions is demonstrated in all cases. Finally, we discuss convergence criteria for judging the quality of the Monte Carlo predictions.

## 2. THEORY

In this section, we discuss the theoretical foundations for the method. This includes the use of the Gaussian copula [15] to generate correlated field realizations, as well as the application of Monte Carlo ray tracing to propagate a given field realization from the source plane to the observation plane.

### A. Random Source Generation

We first describe the synthesis of a random source using a Gaussian copula. The word “copula” is from the Latin meaning to “bond.” In the context of probability theory it has come to be defined as a function that links individual marginal distributions into a joint, multivariate distribution. The basis for this idea is Sklar's theorem [15], which states that given a joint (cumulative) distribution function, $H(x,y)$, and the marginal (cumulative) distribution functions, $F(x)$ and $G(y)$, there exists a copula, $C$, such that

$$H(x,y) = C[F(x), G(y)]. \tag{1}$$

The copula plays the role of linking two marginal distribution functions into a prescribed joint distribution function. Sklar's theorem further states that if the distribution functions are continuous, then the copula is unique.

In the material that follows, we make use of a Gaussian copula (there are many other types [15]) to correlate two initially statistically independent uniformly distributed random variables (RVs) and to subsequently use these correlated samples to create sequences of correlated field realizations.

**1. Generation of Correlated Phase—**We begin with two uniformly distributed, statistically independent RVs, $X_1$ and $X_2$. From this pair, the Box–Muller transformation [16] produces a new pair of RVs,

$$\begin{aligned} Y_1 &= \sqrt{-2\ln X_1}\cos(2\pi X_2), \\ Y_2 &= \sqrt{-2\ln X_1}\sin(2\pi X_2), \end{aligned} \tag{2a}$$

that are jointly normal, i.e., their joint probability density function is

$$\begin{aligned} f_{Y_1,Y_2} &= \tfrac{1}{2\pi}\exp\left\{-\tfrac{1}{2}\left(y_1^2+y_2^2\right)\right\} \\ &= \tfrac{1}{\sqrt{2\pi}}\exp\left\{-\tfrac{1}{2}y_1^2\right\}\tfrac{1}{\sqrt{2\pi}}\exp\left\{-\tfrac{1}{2}y_2^2\right\}, \end{aligned} \tag{2b}$$

and because this joint distribution factors, they are statistically independent. Next, we make use of the following scaling and rotation operations,

$$\begin{vmatrix} Z_1 \\ Z_2 \end{vmatrix} = \frac{1}{\sqrt{2}} \begin{vmatrix} 1 & -1 \\ 1 & 1 \end{vmatrix} \begin{vmatrix} \sqrt{1+r} & 0 \\ 0 & \sqrt{1-r} \end{vmatrix} \begin{vmatrix} Y_1 \\ Y_2 \end{vmatrix}, \tag{3}$$

NIH-PA Author Manuscript

NIH-PA Author Manuscript

NIH-PA Author Manuscript

to find that the RVs, $Z_1$ and $Z_2$, are bivariate normal with correlation coefficient $r$:

$$f_{Z_1 Z_2} = \frac{1}{2\pi\sqrt{1-r^2}} \exp\left\{-\frac{1}{2(1-r^2)}\left(z_1^2 - 2rz_1z_2 + z_2^2\right)\right\}. \tag{4}$$

The Box–Muller transformation and the scaling and rotation constitute the copula that links the marginal distributions on $X_1$ and $X_2$ into the bivariate distribution on $Z_1$ and $Z_2$. Finally, we make use of the percentile transformation [16]

$$T_1 = F_Z(Z_1); \qquad T_2 = F_Z(Z_2), \tag{5}$$

where $F_Z$ is the normal cumulative distribution function. From these operations we obtain the RVs, $T_1$ and $T_2$, which are uniformly distributed on the unit interval and are no longer statistically independent but have correlation coefficient, $r$.

**2. Generation of Correlated Field Realizations—**Having presented a method by which one can obtain a pair of uniformly distributed random variables with arbitrary correlation coefficient, we now describe a process for the generation of correlated field realizations.

A spatially band-limited random field realization [17,18] can be synthesized easily by the following algorithm: Create an $L \times L$ element matrix of zeros and fill the central circular region of diameter $K$ elements with complex numbers of unit amplitudes and phases uniformly distributed over $(0,2\pi)$. Upon Fourier transforming the $L \times L$ array, one arrives at a synthetic field pattern having a Rayleigh probability distribution. The ratio of $L$ to $K$ sets the length of the spatial autocorrelation of the field realization. For example, if $L$=2 K, the Nyquist criterion is met and the length of the autocorrelation is on the order of two pixels.

Use of the phases $\phi_1 = 2\pi m t_1$, $\phi_2 = 2\pi m t_2$ in this procedure, where $t_1$ and $t_2$ are uniformly distributed samples (instantiations of the corresponding RVs, $T_1$ and $T_2$) as in the preceding discussion, and $m$ is a real constant, produces a pair of correlated field realizations. The actual correlation between these two realizations, from the complex Gaussian moment theorem [2], is given by

$$\mu = \exp\left(-\frac{1}{2}\sigma_{\Delta\phi}^2\right), \tag{6}$$

where $\sigma^2_{\Delta\phi} = \mathrm{var}(\phi_1 - \phi_2)$ is the variance of the phase difference.

From the preceding, we observe that for a specified correlation of $r$=1, the resulting phases are perfectly correlated and as a result, the two field realizations are identical. When $r$=0 the phases are uncorrelated and so too are the resulting field realizations. Finally for $r$=−1 the realizations are perfectly anticorrelated. In other words, we generate a pair of field realizations that evolve from perfect correlation to perfect anticorrelation. Our real interest, however, is in the evolution of $Z_1$ from $Y_1$ to $-Y_2$ or of $Z_2$ from $Y_1$ to $Y_2$. For that we need to know the relationship between the specified correlation between $T_1$ and $T_2$ and the correlation between the realizations in the sequence, e.g., $T_1(1), \ldots, T_1(r), \ldots, T_1(-1)$. We denote the phase realizations in this sequence as $T_{1k}$, $k = 1, 2, \ldots, k_{\max}$. It has been shown [18] that this correlation is given by

$$r_{1k} \equiv \frac{E\{(T_{11} - \mu_{11})(T_{1k} - \mu_{1k})\}}{\sigma_{11}\sigma_{1k}} = \sqrt{\frac{1+r}{2}}, \tag{7}$$

where $\sigma_{ij}^2 = E\{(T_{ij} - \mu_{ij})^2\}$ and that the variance of the phase difference is

$$\mathrm{var}(\phi_1 - \phi_2) = (2\pi m)^2 (1 - r_{1k})/6, \tag{8}$$

so that the field correlation coefficient is given by [see Eq. (6)]

NIH-PA Author Manuscript

NIH-PA Author Manuscript

NIH-PA Author Manuscript

$$\mu_{1k}=\exp\left[-\frac{(2\pi m)^2}{12}(1-r_{1k})\right], \tag{9}$$

where we have denoted explicitly that the field correlation is referenced to the first realization in the sequence. For a specified (phase) correlation of

$$r=\cos\left(\pi\frac{k-1}{k_{\max}-1}\right), \tag{10}$$

we then obtain the model-based estimate of the field correlation coefficient

$$\mu_{1k}=\exp\left\{-\frac{(2\pi m)^2}{6}\sin^2\left[\frac{\pi}{4}\left(\frac{k-1}{k_{\max}-1}\right)\right]\right\}, \tag{11}$$

with a fixed incremental correlation of $\mu_{k,k+1}\approx 1-(2m/k_{\max})^2$.

For this field generation algorithm, the roles of the function $r$ [Eq. (10)] and the parameter $m$ are clear. The functional form of $r$ sets the manner in which the field realizations decorrelate. For the form shown in Eq. (10), the decorrelation steps are equal and the choice of the reference is arbitrary; the form of the field correlation coefficient [Eq. (9)] is the same regardless of whether the reference is the first realization or the last. The size of the parameter $m$ dictates how quickly the field patterns decorrelate.

This process leads to the generation of a spatiotemporal field realization cube as illustrated in Fig. 1(a). These two-dimensional speckle fields evolve between the two limits in a prescribed fashion at a specified rate. As such, this evolving speckle field might serve as a realistic model of the temporal behavior of laser illumination scattered by a biological medium [19]. For the purpose of the subsequent simulation discussed herein, however, we choose a different interpretation. Specifically, we interpret the time axis as a spatial dimension and the $x$ and $y$ dimensions as designations of unique ensemble members of a stochastic process. In other words, for a given $x$ and $y$, the third dimension specifies the spatial distribution of a realization of a random line source. This reinterpretation is illustrated in Fig. 1(b). These realizations, illustrated notionally in Fig. 2, have the proper first- and second-order statistics and are smooth and continuous.

With this algorithm, we have generated a stochastic line source with Gaussian correlation given by Eq. (11). In symmetric form this expression is

$$\begin{aligned}\mu_{k_c-k,k_c+k} &\equiv \frac{\langle U_{k_c-k}U^*_{k_c+k}\rangle}{\langle|U_{k_c-k}|^2\rangle^{1/2}\langle|U_{k_c+k}|^2\rangle^{1/2}}\\ &=\exp\left\{-\frac{(2\pi m)^2}{6}\sin^2\left[\frac{\pi}{4}\left(\frac{2k}{k_{\max}-1}\right)\right]\right\},\end{aligned} \tag{12}$$

where $k_c$ is the central position of the line source, the angle brackets indicate a (statistical) average over the ensemble of field realizations, and the asterisk indicates the complex conjugate.

## B. Physical Optics Propagation

For simple geometries, the propagation of the optical field can be performed using physical optics. The basis for the technique is the Huygens–Fresnel principle, which is expressed in two-dimensional form as [20]

$$U_o(x_o)=\frac{i\pi}{\lambda}\int_{-\infty}^{\infty}U_s(x_s)\frac{z}{r_{os}}H_1^{(1)}(kr_{os})\,\mathrm{d}x_s, \tag{13a}$$

where $H^1_{(1)}$ is the Hankel function of the first kind and order one,

NIH-PA Author Manuscript

NIH-PA Author Manuscript

NIH-PA Author Manuscript

$$r_{os}=\left[(x_0-x_s)^2+z^2\right]^{1/2}, \tag{13b}$$

and the *s* and *o* subscripts refer, respectively, to the source and the observation plane. Equation (13a) is also known as the first Rayleigh–Sommerfeld diffraction integral. It has several approximations for different propagation regimes, including the Fresnel and Fraunhofer (far-field) approximations. Taking the Fourier transform of both sides of Eq. (13a), we find the following frequency domain representation for the field in the observation plane:

$$\tilde{U}_o(f_x)=\tilde{U}_s(f_x)\,H(f_x,z), \tag{14a}$$

where

$$H(f_x,z)=\exp\left\{iz\left[k^2-(2\pi f_x)^2\right]^{1/2}\right\} \tag{14b}$$

is the free-space transfer function. Performing a binomial expansion of the square root in Eq. (14b) and keeping only the first two terms yields the Fresnel approximation of the transfer function, i.e.,

$$H(f_x,z)=\exp\left(ikz-i\pi\lambda z f_x^2\right). \tag{15}$$

A random field is characterized by its statistical moments. The first two of these, the intensity and the complex coherence factor, are given by [2]

$$\begin{aligned} I(x) &= \langle |U(x)|^2\rangle, \\ \mu(\Delta x) &= \frac{\langle U(x-\Delta x/2)U^*(x+\Delta x/2)\rangle}{\langle |U(x-\Delta x/2)|^2\rangle^{1/2}\langle |U(x+\Delta x/2)|^2\rangle^{1/2}}. \end{aligned} \tag{16}$$

The coherence length is defined by

$$d_c=\int_{-\infty}^{\infty}|\mu(\Delta x)|\,\mathrm{d}\Delta x. \tag{17}$$

Each realization of the random source can be propagated using Eq. (13a) and (13b) and the resulting ensemble averaged (as above) to obtain the intensity and the complex coherence factor. Alternatively, under certain weak restrictions on the propagation distance, the statistical moments in the source and observation planes can be related through the generalized van Cittert–Zernike theorem [21], viz.,

$$\begin{aligned} I_o(x_o) &\propto \int_{-\infty}^{\infty}\mu_s(\Delta x_s)\exp\{i2\pi x_o\Delta x_s/\lambda z\}\,\mathrm{d}\Delta x_s \\ \mu_o(\Delta x_o) &\propto \int_{-\infty}^{\infty}I_s(x_s)\exp\{i2\pi x_s\Delta x_o/\lambda z\}\,\mathrm{d}x_s. \end{aligned} \tag{18}$$

The generalized van Cittert–Zernike theorem applies to quasi-homogeneous random sources. These are sources for which the correlation function depends only on the absolute separation of the source points and the correlation function varies much more quickly (i.e., it is a faster function) than the intensity distribution [1].

### C. Monte Carlo Propagation

Monte Carlo refers to a technique first proposed by Metropolis and Ulam to simulate physical processes using stochastic modeling [22]. In radiative transport applications, the Monte Carlo technique involves tracing rays of light through a medium as they are scattered and absorbed. At each scattering interaction, a new random direction is selected based on the single-scattering phase function of the medium at that location. Monte Carlo modeling is popular because it is simple and easily adapted to odd geometries and boundary conditions [6,7,23–27]. Its primary disadvantage (computation time) has been largely mitigated by increases in computer speed. Another disadvantage is that most Monte Carlo light-propagation codes tend to track just the intensity of the field. More recently, Monte Carlo techniques have been adapted to model

NIH-PA Author Manuscript

NIH-PA Author Manuscript

NIH-PA Author Manuscript

polarization [28–33] by keeping track of changes in the polarization of light as it is scattered. It has also been used to model phase, in optical coherence tomography for instance, by keeping track of the distance (time) traveled by an interrogating light pulse, which is mathematically interfered with a reference beam [11,12,34–37].

This work describes a new Monte Carlo technique for propagating optical fields. It is based on the Huygens–Fresnel principle: Each point on a wavefront is considered to be the source of a cylindrical wave (known as a Huygens wavelet) emanating from that point [see Eq. (13a)]. Monte Carlo sampling of the Huygens wavelets involves launching multiple rays from the center of each wavelet and tracking the change in phase of each ray before it reaches the observation plane. For example, a partially coherent source field is propagated using multiple Huygens wavelets emanating from different points across a given source realization. The initial amplitude and phase of each wavelet are determined by the source strength at that point. When a given ray reaches the observation plane, it is added coherently to all those that have reached the same location.

**1. Source Sampling—**We assume that a typical source realization is a line source having $n_s$ elements (i.e., it is a linear array); each source realization is a horizontal line (sample) from the cube in Fig. 1(b). A given source realization is propagated by launching rays (with random directions) uniformly over a semicircle centered on each source element (see Fig. 3). This is equivalent to sampling the Huygens wavelets emanating from each source element. Each ray is launched with an initial phase and amplitude specified by the field for that source element.

When a physical structure is interposed between source and detector, e.g., an aperture, the rays are traced to the aperture and the phase is adjusted according to the distance traveled. Subsequently, the phase and amplitude are modified by the complex transmission function at the point in the aperture at which the ray hits. For the simulations in this paper, the imaginary part of this transmittance function is always zero. The slit is modeled as having unit amplitude for all elements that constitute the interior and zero amplitude elsewhere. The Fresnel zone plate was modeled using an array of 5,000 elements uniformly distributed across the plate of diameter 50λ. Each element of the plate is assigned an amplitude of zero or one depending on whether the physical location of that element blocks or passes the ray.

Finally, the field is propagated from the secondary source plane (i.e., the aperture) to the observation plane by again launching rays (randomly) over semicircles centered on each secondary source element (i.e., sampling each secondary source Huygens wavelet). For efficiency reasons, all rays launched from the source are constrained to fall within the aperture (i.e., no rays that would miss the aperture are propagated). Similarly, all rays leaving the aperture reach the detector. The total number of rays launched per realization is divided evenly among the $n_s$ points of the realization array to ensure uniform sampling of the source wavefront.

**2. Coherent Summation—**Consider a ray arriving at a detector of finite physical size (a bin or pixel) in the observation plane. The state of the ray at the intersection point on this plane depends on the distance that the ray has traveled, $l_j$. If the ray starts with an initial amplitude and phase represented by $A_j \exp(i\phi_j)$, then its final value will be

$$B_j e^{i\beta_j} = A_j e^{-\mu_a l_j} e^{i(\phi_j + k l_j)}, \tag{19}$$

where $\mu_a$ is the absorption cross section per unit volume and $k$ is the wavenumber. Now another ray may eventually reach a point within this same pixel from a different starting position and have a different optical path length. If a number of rays reach the same ($n$th) bin, then the coherent ray sum at the point $x_n$ in the observation plane will be

NIH-PA Author Manuscript

NIH-PA Author Manuscript

NIH-PA Author Manuscript

$$U(x_n) = \sum_j B_j e^{i\beta_j} = \sum_j A_j e^{-\mu_a l_j} e^{i(\phi_j + k l_j)}. \tag{20}$$

For the case of free-space (no absorption or scattering) propagation between two parallel planes separated a distance $d$, this simplifies to

$$U(x_n) = \sum_j A_j e^{i(\phi_j + k l_j)}, \qquad l_j = \frac{d}{\cos\theta_j}, \tag{21}$$

and $\theta_j$ is the impact angle of the ray.

**3. Observation Plane Sampling—**The observation plane sampling must be performed such that competing constraints are simultaneously satisfied. The first constraint on the sampling is that the sample size (i.e., pixel or bin size) be large enough to achieve sufficient Monte Carlo signal statistics (i.e., that the variance in the Monte Carlo estimate be minimized). In effect, having larger bins increases the number of rays per bin and decreases the variance. On the other hand, the bin size must also be smaller than the speckle size so that the rays can be coherently summed. This is generally not a problem for free-space diffraction geometries but would need to be taken into account when investigating propagation through multiple-scattering media. In fact, it has been shown that in this case, the bin size must be on the order of the wavelength of the light [14]. Finally, while it is not a hard constraint, the bin size should also be small enough that spatial resolution is not compromised.

## 3. RESULTS

Three specific cases were treated. The first (Fig. 4) was of a point source (by definition perfectly coherent) imaged by a binary Fresnel zone plate. This case was intended to validate the assertion that Monte Carlo techniques are capable of modeling interference phenomena, viz., diffraction. The second case (Fig. 5) was of a partially coherent source and free-space propagation to an observation plane at the Rayleigh distance. Such a case conforms to the requirements of the generalized van Cittert–Zernike theorem. Monte Carlo and physical optics calculations are compared with each other and with the predictions based on this theorem. The third case (Fig. 6) was identical to the second except that an aperture was placed midway between the source and observation planes. This case simulates a secondary source that does not conform to the usual quasi-homogeneous source description and demonstrates the well-known concept that restricting the angular extent of the source increases its spatial coherence. Monte Carlo and physical optics predictions are compared.

### A. Fresnel Zone Plate (Coherent Propagation)

For this case, a point source was imaged by a binary Fresnel zone plate. Source and image distances were each 100λ. The zone plate was 50λ in diameter with a central (clear) zone of 14λ diameter. Results of the Monte Carlo and physical optics calculations are compared in Fig. 7. The nonparaxial (wide angle) physical optics calculations were carried out by numerically integrating the secondary source Huygens wavelets in the plane of the Fresnel zone plate. Good agreement between the physical optics and Monte Carlo calculations is seen for the central lobe, with minor differences between the two methods in the wings. The distribution in the observation plane is effectively the square of the point-spread function of the zone plate.

### B. Free-Space Propagation (Partially Coherent Propagation)

For this case, a random source was propagated to an observation plane located at the Rayleigh distance. Source realizations were generated using the algorithm outlined in Section 2, with cube dimensions of 256×256×51, a spatial sampling factor of $L/K$=4 (i.e., twice Nyquist), and

NIH-PA Author Manuscript

NIH-PA Author Manuscript

NIH-PA Author Manuscript

a correlation parameter of $m$=5. Incremental correlation steps as described in Eq. (11) were used. Reinterpretation of the field cube in terms of a stochastic process leads to an ensemble of $256^2$ line source realizations, each having a length of 51 elements. Source elements were assumed to be 4λ in length.

Shown in Fig. 8 is the source plane field characterization as computed over the ensemble of $256^2$ realizations. Figure 8(a) is intensity and Fig. 8(b) is the real part of the complex coherence factor. For the statistically symmetric source and the physically symmetric architectures studied herein, the imaginary part of the complex coherence factor is zero. The actual source length was 204λ, and its effective length [using a definition similar to Eq. (17)] was 69.8λ. Free-space propagation to the observation plane located at the Rayleigh range [$z_R/\lambda = l^2/\lambda^2 = (204)^2$] was performed using a fast Fourier transform (FFT) implementation of Eqs. (14a) and (14b). Each source realization was individually Fourier transformed, multiplied by the free-space transfer function [Eq. (14b)] and inverse Fourier transformed to yield a member of the ensemble of observation plane realizations. Figure 9 illustrates the resulting intensity and complex coherence factor in the observation plane. The effective image length and coherence length were 983λ and 684λ, respectively. The intensity and the complex coherence factor were also computed on the basis of the generalized van Cittert–Zernike theorem. Disagreement between the two predictions for the intensity in Fig. 9(a) is a reflection of the fact that the complex coherence factor is not substantially narrower than the intensity (as is the case for a true quasi-homogeneous source) but has a small, nonzero value at the edge of the source [see Fig. 8(b)]. As a result of the truncated source coherence factor (product of the actual coherence function and a rect function [38]), its transform is convolved with a sinc function, thus producing the undulations seen in Fig. 9(a). Shown in Fig. 10 is a comparison of the Monte Carlo and physical optics calculations. Physical optics and Monte Carlo predictions for the intensity agree quite well, with absolute residuals between the two calculations of less than 0.002. Agreement for the complex coherence factor is also quite good, with absolute residuals between the two calculations of less than 0.003.

### C. Intermediate Aperture (Partially Coherent Propagation)

Calculations also were performed for the case when an intermediate aperture (half the size of the source) is present and located half-way between the source and observation planes (see Fig. 6). Physical optics calculations utilized the same FFT algorithm as for the free-space architecture. Each source realization was propagated to the aperture plane in the manner described above, the Kirchhoff boundary conditions of the aperture applied, and the realization then propagated to the observation plane. Results are shown in Fig. 11. Intensities predicted by physical optics and Monte Carlo agree very well, with an absolute residual of less than 0.005. Note that the diffraction patterns do not come fully to zero outside the central lobe as would be expected in the case of a fully coherently illuminated aperture. Results for the complex coherence factor agree closely as well. Within a region of the first null in the diffraction pattern, the absolute residual in the two estimates of the complex coherence function are within approximately 0.01. The ripple structure is interesting and arises because of the statistical behavior of the secondary source; it is intermediate between the fully coherent and quasi-homogeneous cases.

### D. Convergence of the Calculations

Here we address the (convergence) issue of how many rays must be traced per field realization, and how many realizations must be propagated to obtain realistic firstand second-order field statistics. We use as a global measure of fidelity the *RMS* error between the Monte Carlo predictions of the intensity and complex coherence factor and the corresponding moments based on physical optics and computed over all the realizations. Thus for the two statistics,

NIH-PA Author Manuscript

NIH-PA Author Manuscript

NIH-PA Author Manuscript

intensity and complex coherence factor, we compute the measures of convergence [with respect to the fully converged physical optics results, $I_{PO}(x_i)$ and $\mu_{PO}(x_i)$],

$$RMS_I(N_r,N) = \sqrt{\frac{1}{n_o}\sum_{i=1}^{n_o}[I_{MC}(x_i,N_r,N) - I_{PO}(x_i)]^2},$$
$$RMS_\mu(N_r,N) = \sqrt{\frac{1}{n_o}\sum_{i=1}^{n_o}[\mu_{MC}(x_i,N_r,N) - \mu_{PO}(x_i)]^2}, \quad (22)$$

where the summation is over the observation plane and we have explicitly denoted the dependence on the total number of rays per realization, $N_r$, and the number of realizations, $N \leq N_{total}$, where $N_{total}$ is the total number of realizations in the experiment. Within each square-bracketed term, the Monte Carlo estimates contain fluctuations due to the number of samples and due to the number of realizations. These fluctuations are of course statistically independent, and as a result, the corresponding variances add.

Inspection of these two metrics calculated over all the realizations, $RMS_I(N_r,N_{total})$ and $RMS_\mu(N_r,N_{total})$, shows the expected dependence on number of rays per realization, $1/\sqrt{Nr}$. Interestingly, when the number of rays propagated per realization is sufficiently low, the two metrics $RMS_I(N_r,N)$ and $RMS_\mu(N_r,N)$ display a $1/\sqrt{N}$ dependence on the number of realizations. In this case, the fluctuations due to sampling outweigh those due to the statistical field variations.

In the intermediate regime, where the number of rays per realization provides an increasingly faithful estimate of the individual realizations, the behavior of the convergence metrics is more complex. In such a case, the *RMS* errors computed on the initial fraction of the ensemble members continue to display the $1/\sqrt{N}$ dependence on the number of realizations, but thereafter, the convergence displays a much more rapid exponential behavior.

The above discussion dealt with global measures of fidelity. Local measures also can be explored. For each of the architectures explored herein, the observation plane field is a circular complex Gaussian random process. As such, the intensity at any point in the observation plane should display exponential statistics. In other words, for an arbitrary point in the observation plane, the probability distribution of the intensity (computed over the members of the ensemble) should be exponential. It is characteristic of such a distribution that the standard deviation is equal to the mean. For example, it is commonly accepted that the statistical contrast (defined as the quotient of the standard deviation and the mean) for a polarized, fully developed speckle pattern is unity [17]. Thus, for the Monte Carlo calculations, any departure from this unity contrast is due to under sampling. This argument is based on the observation that for an arbitrary point in the observation plane, the intensity fluctuations possess two components, one intrinsic to the random process and one associated with inaccuracies due to the Monte Carlo sampling. Of course these two random fluctuations are statistically independent, and as a result, their variances are additive. A simple test for adequate Monte Carlo sampling for the intensity is therefore to inspect the pointwise contrast (quotient of the standard deviation and the mean computed over the entire ensemble). If this departs substantially from unity at any point in the observation plane, then a greater degree of sampling is indicated. As an example, Fig. 12(a) is a display of the contrast for the intermediate aperture case. Results for the physical optics and Monte Carlo calculations are shown along with the theoretical value of unity for an exponential distribution. Maximum departures from the theoretical value of unity for physical optics and Monte Carlo are, respectively, 0.013 and 0.087. Shown in Fig. 12(b) is the excess contrast due to Monte Carlo sampling (MC contrast –PO contrast) along with the corresponding intensity pattern.

Local measures of the convergence for the complex coherence factor can be derived through inspection of the field product in the numerator [see Eq. (16)]. Although this field product is

NIH-PA Author Manuscript

NIH-PA Author Manuscript

NIH-PA Author Manuscript

not generally exponential, its conditional statistics are. Specifically, for a given separation, if the samples are segregated into positive and negative subsets, each subset displays an exponential distribution. Separate contrast convergence criteria, as above, then can be applied to each to arrive at a composite convergence criterion.

Note that convergence of the Monte Carlo estimates for intensity and those for the complex coherence factor differ somewhat. Residual errors in the estimates of the intensity for the free-space and intermediate aperture configu-rations [Figs. 10(a) and 11(a)] were very similar. Residuals for the complex coherence factors [Figs. 10(b) and 11(b)], however, were different, with the estimate for the free-space case being much more accurate. This can be understood in light of the fact that for the free-space configuration, the intensity pattern in the observation plane is wider than the coherence length. Higher field values provide better estimates of the complex coherence function (see Fig. 12), even though the coherence may be low. On the other hand, for the intermediate-aperture case, the coherence function is wider than the intensity pattern. In particular, for regions in which the intensity is low, estimates of the complex coherence factor depart somewhat from the physical optics predictions. It is in regions of low intensity that the estimate of the complex coherence factor is most sensitive to the number of rays propagated. Note that regions of lower intensity are not caused by the arrival of fewer rays. Rather, they are caused by destructive interference. However, these regions of lower and higher intensity do display different statistics, caused by a different proportion of fluctuations due to the intrinsic fluctuations of the field and those due to the Monte Carlo sampling.

## 4. DISCUSSION AND CONCLUSIONS

Modeling the effects of spatial coherence in simple optical systems, such as two-dimensional diffracting structures and weakly scattering media, is straightforward, if not simple [1–3,5]. The literature abounds with analytic modeling of the effects, their experimental verification, and methods for numerical calculations. Of particular note is the body of work on atmospheric propagation of light [4,39,40]. On the other hand, the description of spatial coherence effects in more complex systems, such as multiply scattering media, is very difficult. As a result, such phenomena have until fairly recently been ignored. Nevertheless, spatial coherence effects are of obvious importance, for example in a number of biomedical imaging modalities such as optical coherence tomography and confocal microscopy. Our ultimate objective therefore is to account for these coherence effects. We believe such efforts will lead to a more comprehensive understanding of propagation effects in multiple scattering media and to better instrumentation and new data acquisition modalities.

In this paper, we have taken the initial steps toward a quantitative description of spatial coherence effects in complex optical systems. We have demonstrated a means of generating realizations of physically realistic random sources having arbitrary coherence properties. We have shown that with straightforward modifications to traditional Monte Carlo ray-tracing methods, diffraction effects can be predicted and that these predictions agree well with physical optics calculations. Finally, we have demonstrated generation of partially coherent field realizations that are not subject to the quasi-homogeneous source approximation.

Continuing research efforts are aimed at generalizing the concept of the copula algorithm to provide two-dimensional field realizations and developing structured multiple scatter models of the propagation medium. The simulations presented herein are of a line source and thus cannot account for polarization effects. The two-dimensional generalization will provide a means of simulating the full wave nature of the field. Although the copula concept was used here to model stochastic sources, it is of obvious use for generating fully stochastic propagation media as well.

NIH-PA Author Manuscript

NIH-PA Author Manuscript

NIH-PA Author Manuscript

## ACKNOWLEDGMENT

This work was sponsored in part by National Institutes of Health (NIH) grant CA103824.

## REFERENCES

1. Wolf, E. Introduction to the Theory of Coherence and Polarization of Light. Cambridge U. Press; 2007.
2. Goodman, JW. Statistical Optics. Wiley; 1985.
3. Fischer DG, Wolf E. Inverse problems with quasi-homogeneous random media. J. Opt. Soc. Am. A 1994;11:1128–1135.
4. Andrews, LC.; Phillips, RL. Laser Beam Propagation through Random Media. SPIE Press; 1998.
5. Fischer DG, Visser TD. Spatial correlation properties of focused partially coherent light. J. Opt. Soc. Am. A 2004;21:2097–2102.
6. Wilson BC, Adam G. A Monte Carlo model for the absorption and flux distributions of light in tissue. Med. Phys 1983;10:824–830. [PubMed: 6656695]
7. Prahl, SA.; Keijzer, M.; Jacques, SL.; Welch, AJ. A Monte Carlo model of light propagation in tissue. In: Müller, GJ.; Sliney, DH., editors. SPIE Proceedings of Dosimetry of Laser Radiation in Medicine and Biology. SPIE Press; 1989. p. 102-111.Institute Series 5
8. Tsang, L.; Kong, JA.; Ding, KH.; Ao, CO. Scattering of Electromagnetic Waves: Numerical Simulations. Wiley; 2001.
9. Ishimaru, A. *Wave Propagation and Scattering in Random* Media. IEEE; 1997.
10. Tsang, L.; Kong, JA.; Ding, K-H. Scattering of Electromagnetic Waves: Theories and Applications. Wiley; 2000.
11. Xiong G, Xue P, Wu J, Miao Q, Wang R, Ji L. Particle-fixed Monte Carlo model for optical coherence tomography. Opt. Express 2005;13:2182–2195.
12. Tycho A, Jorgensen TM, Yura HT, Andersen PE. Derivation of a Monte Carlo method for modeling heterodyne detection in optical coherence tomography systems. Appl. Opt 2002;41:6676–6691. [PubMed: 12412659]
13. CairnsBAn investigation of radiative transfer and multiple scattering. Ph.D. thesis1992University of Rochester (Available from UMI Dissertation Information Service, 300 N. Zeeb Road, Ann Arbor, Michigan 48106).
14. Mujat C, Dogariu A. Statistics of partially coherent beams: a numerical analysis. J. Opt. Soc. Am. A 2004;21:1000–1003.
15. Nelson, RB. An Introduction to Copulas. Springer-Verlag; 1999.
16. Papoulis, A.; Pillai, SU. Probability, Random Variables, and Stochastic Processes. 4th ed.. McGraw-Hill; 2002.
17. Goodman, JW. Statistical properties of laser speckle patterns. In: Dainty, JC., editor. Laser Speckle and Related Phenomena. Springer-Verlag; 1975. p. 9-75.
18. Duncan DD, Kirkpatrick SJ. The copula: a tool for simulating dynamic speckle. J. Opt. Soc. Am. A 2008;25:231–237.
19. Oulamara A, Tribillon G, Duvernoy J. Biological activity measurement on botanical specimen surfaces using a temporal decorrelation effect of laser speckle. J. Mod. Opt 1989;36:165–179.
20. Stamnes, JJ. Waves in Focal Regions: Propagation, Diffraction, and Focusing of Light, Sound, and Water Waves. Hilger; 1986.
21. Born, M.; Wolf, E. Principles of Optics. 4th ed.. Pergamon; 1970.
22. Metropolis N, Ulam S. The Monte Carlo method. J. Am. Stat. Assoc 1949;44:335–341. [PubMed: 18139350]
23. Keijzer M, Jacques SL, Prahl SA, Welch AJ. Light distributions in artery tissue: Monte Carlo simulations for finite-diameter laser beams. Lasers Surg. Med 1989;9:148–154. [PubMed: 2716459]
24. Wang L, Jacques SL, Zheng L. MCML-Monte Carlo modeling of light transport in multi-layered tissues. Comput. Methods Programs Biomed 1995;47:131–146. [PubMed: 7587160]
25. Moffitt TP, Prahl SA. Sized-fiber reflectometry for measuring local optical properties. IEEE J. Sel. Top. Quantum Electron 2001;7:952–958.

NIH-PA Author Manuscript

NIH-PA Author Manuscript

NIH-PA Author Manuscript


26. Bargo PR, Prahl SA, Jacques SL. Optical properties effects upon the collection efficiency of optical fibers in different probe configurations. IEEE J. Sel. Top. Quantum Electron 2003;9:314–321.
27. Carp SA, Prahl SA, Venugopalan V. Radiative transport in the delta-P1 approximation: Accuracy of fluence rate and optical penetration depth predictions in turbid semi-infinite media. J. Biomed. Opt 2004;9:632–647. [PubMed: 15189103]
28. Cameron BD, Rakovic MJ, Mehrubeoglu M, Kattawar GW, Rastegar S, Wang LV, Coté G. Measurement and calculation of the two-dimensional backscattering Mueller matrix of a turbid medium. Opt. Lett 1998;23:485–487. [PubMed: 18084551]
29. Bartel S, Hielscher AH. Monte Carlo simulations of the diffuse backscattering Mueller matrix for highly scattering media. Appl. Opt 2000;39:1580–1588. [PubMed: 18345055]
30. Xu M. Electric field Monte Carlo simulation of polarized light propagation in turbid media. Opt. Express 2004;26:6530–6539.
31. Côté D, Vitkin IA. Robust concentration determination of optically active molecules in turbid media with validated three-dimensional polarization sensitive Monte Carlo calculations. Opt. Express 2005;13:148–163.
32. Ramella-Roman JC, Prahl SA, Jacques SL. Three Monte Carlo programs of polarized light transport into scattering media: part I. Opt. Express 2005;13:4420–4438.
33. Ramella-Roman JC, Prahl SA, Jacques SL. Three Monte Carlo programs of polarized light transport into scattering media: part II. Opt. Express 2005;13:10392–10405.
34. Smithies DJ, Lindmo T, Chen Z, Nelson JS, Milner TE. Signal attenuation and localization in optical coherence tomography studied by Monte Carlo simulation. Phys. Med. Biol 1998;43:3025–3044. [PubMed: 9814533]
35. Yao G, Wang LV. Monte Carlo simulation of an optical coherence tomography signal in homogeneous turbid media. Phys. Med. Biol 1999;44:2307–2320. [PubMed: 10495123]
36. Lu Q, Gan X, Gu M, Luo Q. Monte Carlo modeling of optical coherence tomography imaging through turbid media. Appl. Opt 2004;43:1628–1637. [PubMed: 15046164]
37. Kirillin MY, Meglinskii IV, Priezzhev AV. Effect of photons of different scattering orders on the formation of a signal in optical low-coherence tomography of highly scattering media. Quantum Electron 2006;36:247–252.
38. Goodman, JW. Introduction to Fourier Optics. 3rd ed.. Roberts; 2005.
39. Gbur G, Wolf E. Spreading of partially coherent beams in random media. J. Opt. Soc. Am. A 2002;19:1592–1598.
40. Roychowdhury H, Ponomarenko SA, Wolf E. Change in the polarization of partially coherent electromagnetic beams propagating through the turbulent atmosphere. J. Mod. Opt 2005;52:1611–1618.

NIH-PA Author Manuscript

NIH-PA Author Manuscript

NIH-PA Author Manuscript

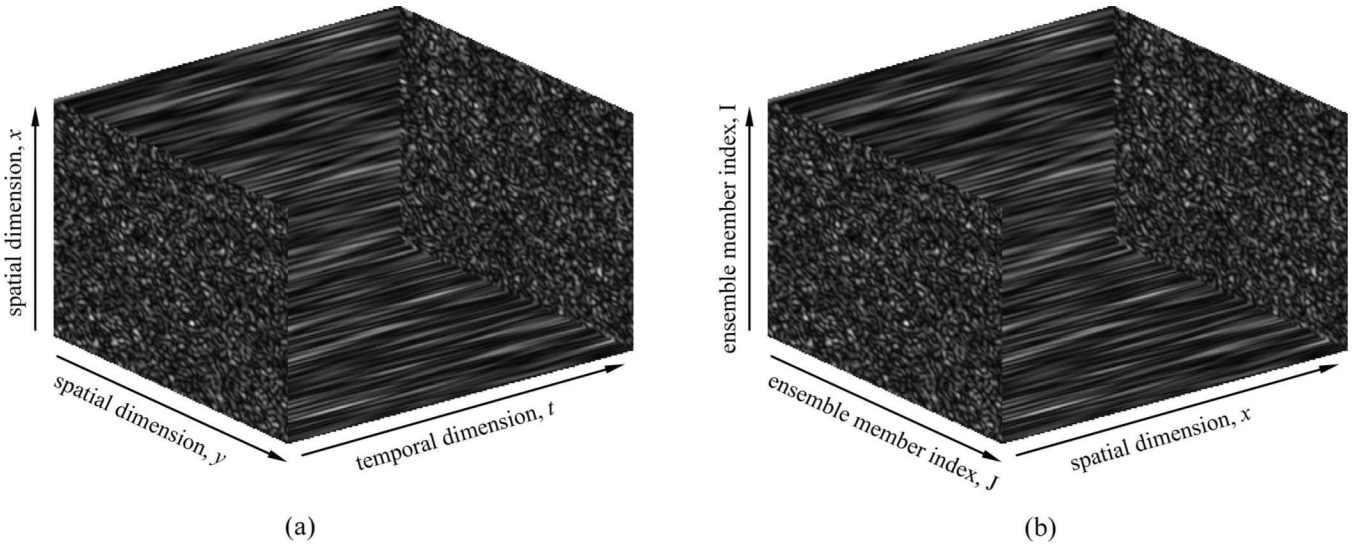


**Fig. 1.**

(a) Illustration of the field realization cube in terms of two spatial and one temporal dimension.

(b) Reinterpretation of the field realization cube in terms of an ensemble of spatial line sources.

NIH-PA Author Manuscript

NIH-PA Author Manuscript

NIH-PA Author Manuscript

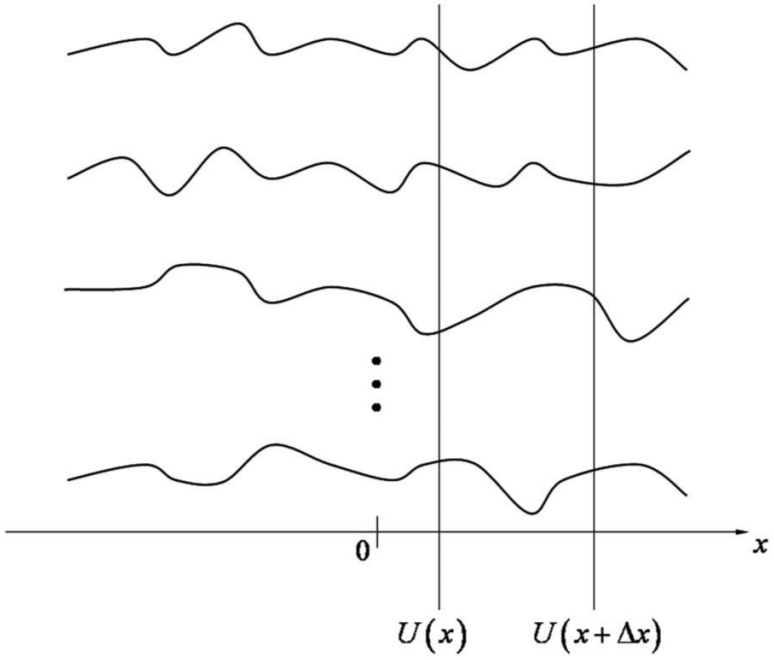


**Fig. 2.**
Ensemble members of the stochastic source field process.

NIH-PA Author Manuscript

NIH-PA Author Manuscript

NIH-PA Author Manuscript

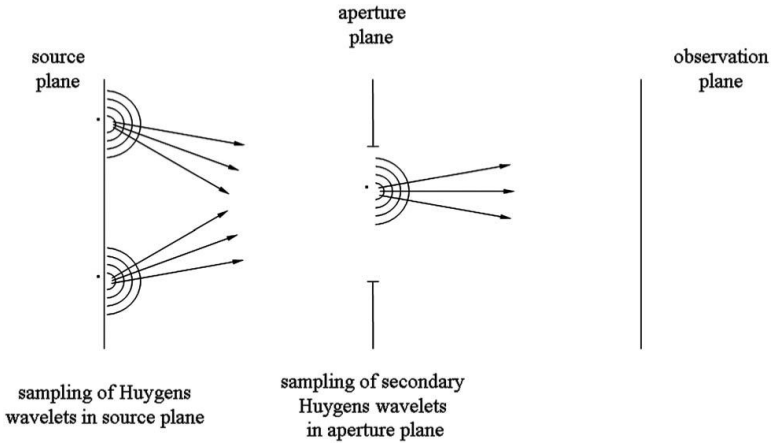


**Fig. 3.**
Illustration of Monte Carlo approximation of the Huygens wavefront.

NIH-PA Author Manuscript

NIH-PA Author Manuscript

NIH-PA Author Manuscript

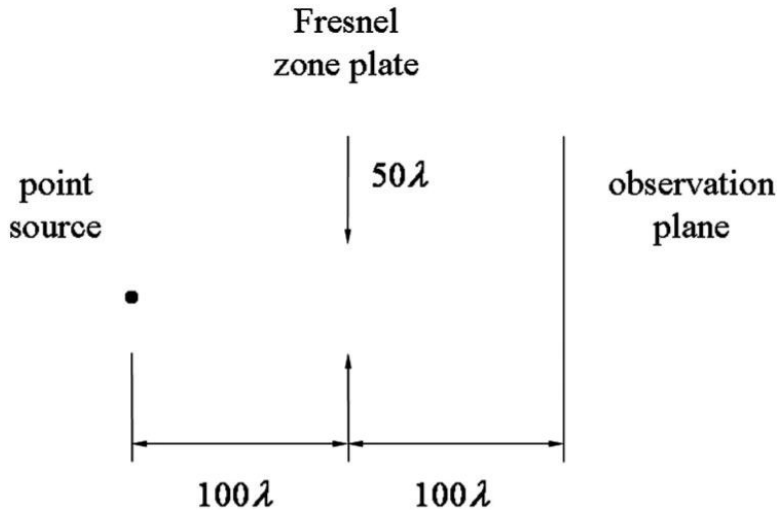


**Fig. 4.**
Illustration of Fresnel zone plate imaging architecture.

NIH-PA Author Manuscript

NIH-PA Author Manuscript

NIH-PA Author Manuscript

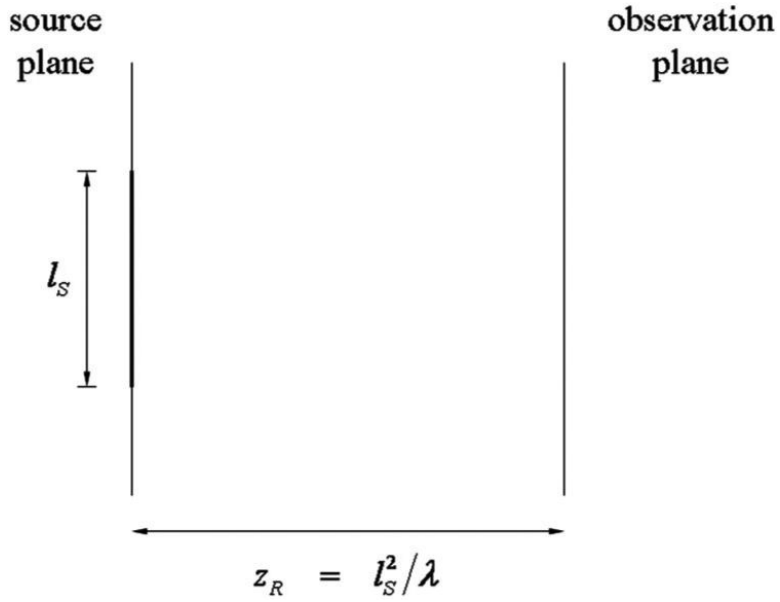


**Fig. 5.**
Free-space architecture.

NIH-PA Author Manuscript

NIH-PA Author Manuscript

NIH-PA Author Manuscript

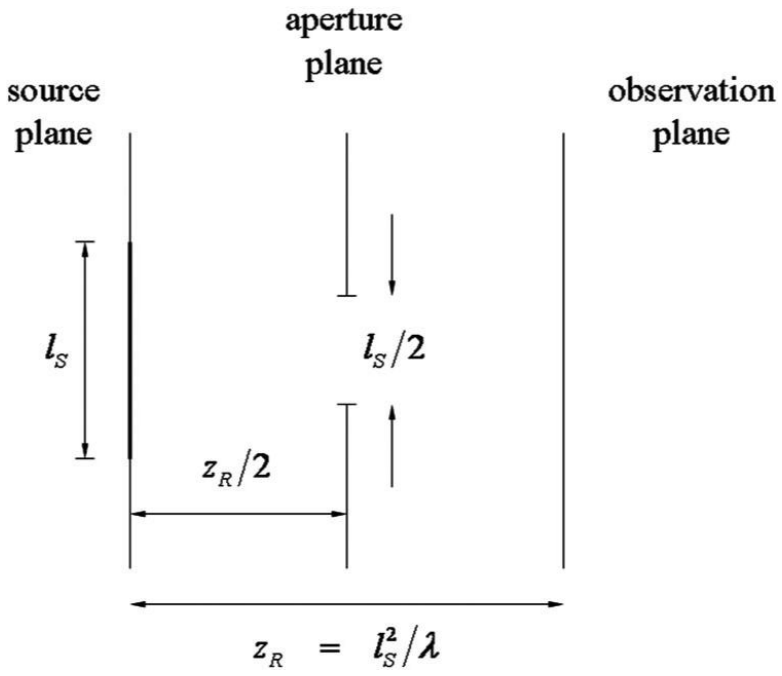


**Fig. 6.**
Alternate simulation configuration with interposed limiting aperture.

NIH-PA Author Manuscript

NIH-PA Author Manuscript

NIH-PA Author Manuscript

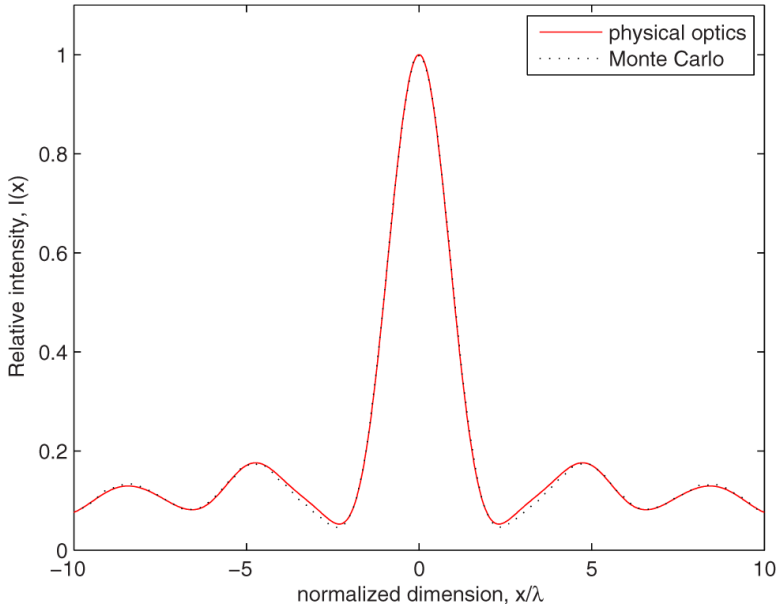


**Fig. 7.**

(Color online) Monte Carlo and physical optics calculation of imaging of the point source with the Fresnel zone plate. The zone plate is 50λ in diameter with a central (clear) zone of 14λ diameter; object and image distances are each 100λ.

NIH-PA Author Manuscript
NIH-PA Author Manuscript
NIH-PA Author Manuscript



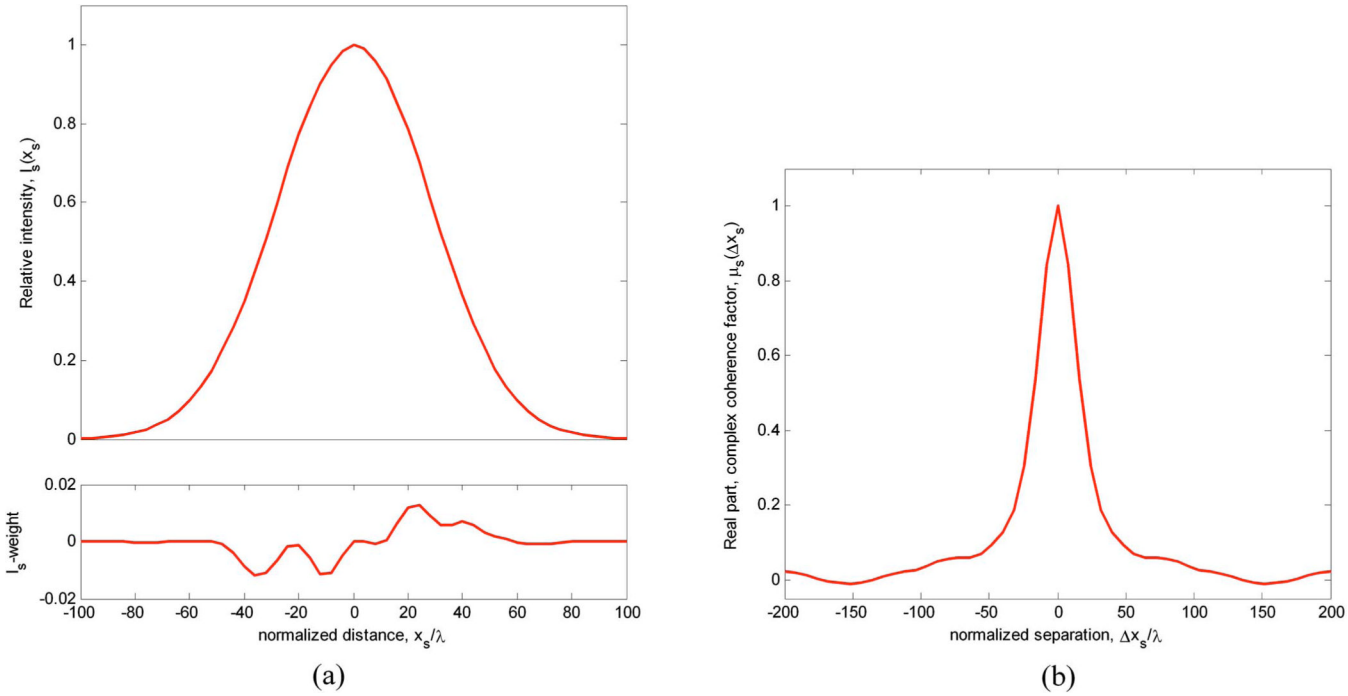


**Fig. 8.**

(Color online) Source plane field characterization calculated over all ensemble members. (a) Intensity, with effective source length $l_s$=69.8λ (residual with respect to Gaussian source weighting shown at bottom); (b) real part of complex coherence factor, with coherence length $d_c$=50.4λ.

NIH-PA Author Manuscript
NIH-PA Author Manuscript
NIH-PA Author Manuscript



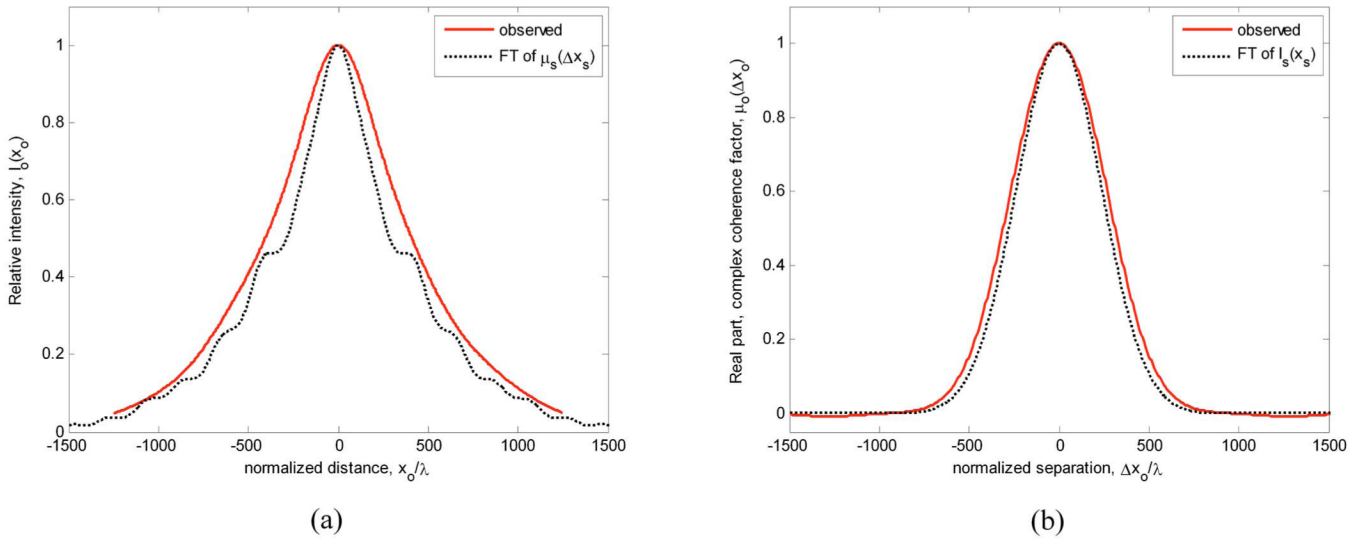


**Fig. 9.**

(Color online) Observation plane field characterization calculated over all ensemble members and as calculated using the generalized van Cittert–Zernike theorem. (a) Intensity with effective length $l_o$=983λ; (b) real part of the complex coherence factor, with coherence length $d_c$=684λ.

NIH-PA Author Manuscript
NIH-PA Author Manuscript
NIH-PA Author Manuscript



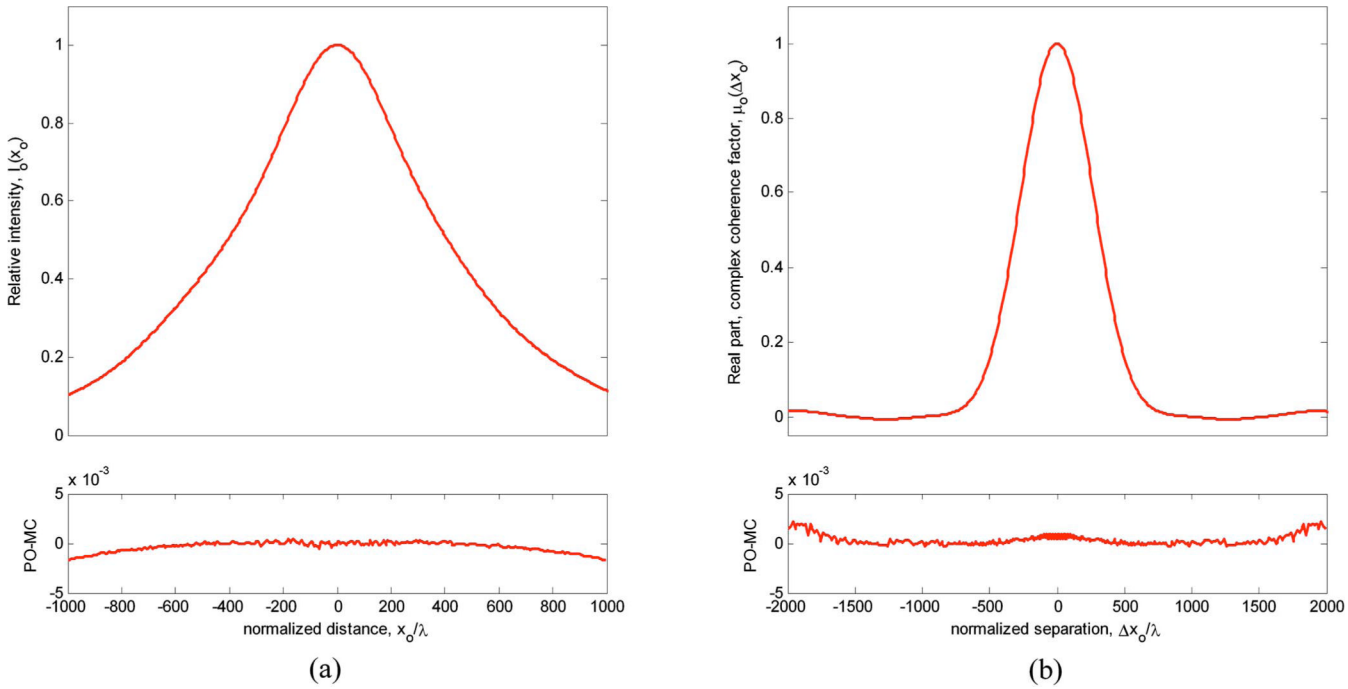


**Fig. 10.**

(Color online) Comparison of Monte Carlo and physical optics results for free-space propagation. Monto Carlo calculations used 50,000 rays/source pixel (2.55 M/realization) and an 8λ observation plane pixel size. In each figure the physical optics calculation is shown at the top with the absolute residual (physical optics–Monte Carlo) shown at the bottom. (a) Intensity, (b) real part of complex coherence factor.

NIH-PA Author Manuscript
NIH-PA Author Manuscript
NIH-PA Author Manuscript



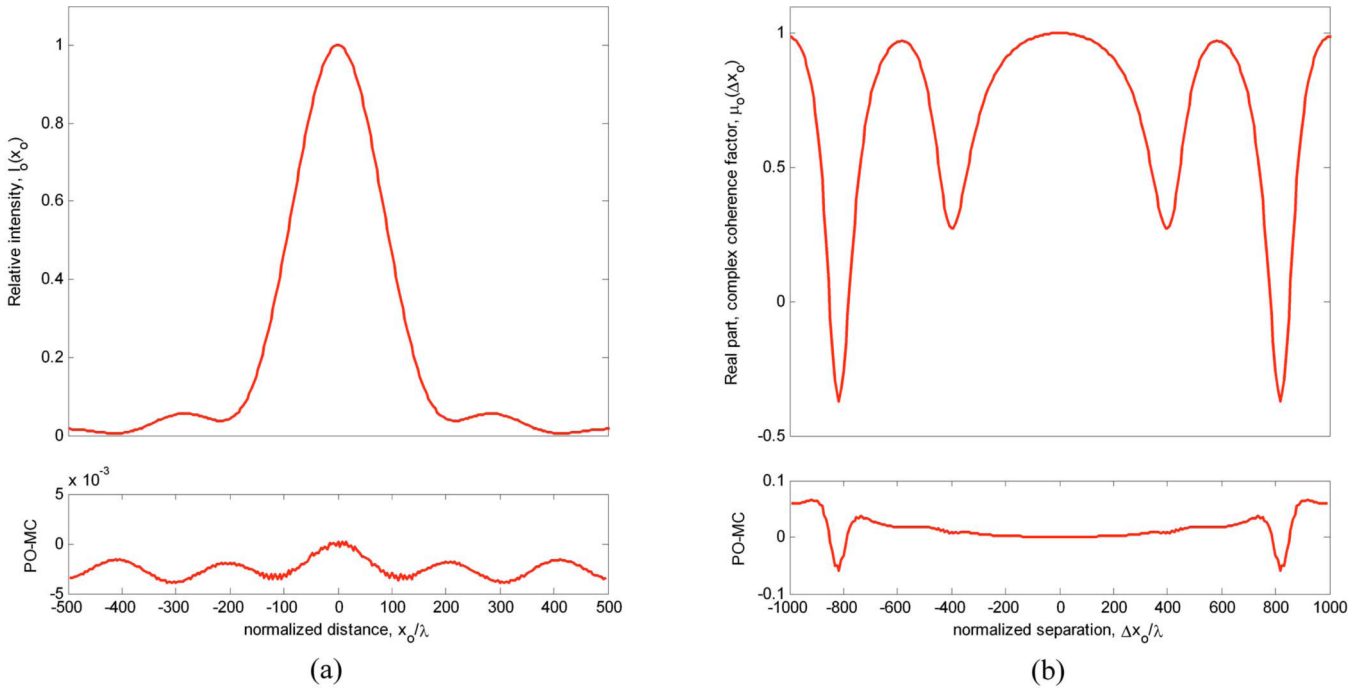


**Fig. 11.**

(Color online) Observation plane field characterization, by physical optics and Monte Carlo calculations, calculated over all ensemble members for configuration shown in Fig. 6. Monte Carlo calculations used 2.58 M rays/realization and a 4λ observation plane pixel size. In each figure the physical optics calculation is shown at the top with the absolute residual (physical optics–Monte Carlo) shown at the bottom. (a) Intensity with effective image length of 221λ, (b) real part of the complex coherence factor.

NIH-PA Author Manuscript
NIH-PA Author Manuscript
NIH-PA Author Manuscript



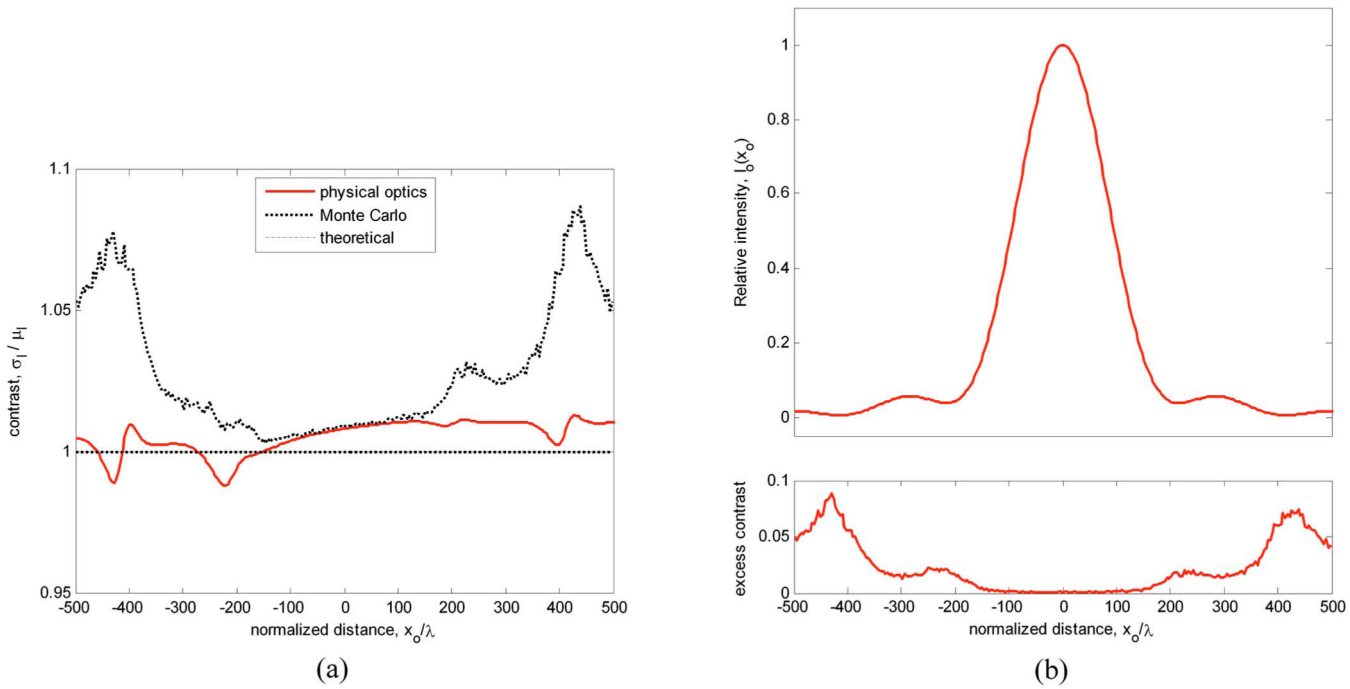


**Fig. 12.**

(Color online) Intensity contrast for the intermediate-aperture configuration. (a) Contrast (as calculated over all ensemble members) for physical optics and Monte Carlo results shown in comparison with theoretical value of unity. (b) Observation plane intensity, top, and excess contrast, bottom (difference between that for Monte Carlo and physical optics).